JOURNAL OF APPLIED ELECTROCHEMISTRY 23 (1993) 1051–1055

# Factors affecting the characteristics of the negative electrodes for nickel–hydrogen batteries

K. NAITO, T. MATSUNAMI, K. OKUNO

*Okuno Chemical Industries Co. Ltd, 1-10-25 Hanaten-Higashi, Tsurumi-Ku, Osaka 538, Japan*

M. MATSUOKA, C. IWAKURA

*Department of Applied Chemistry, College of Engineering, University of Osaka Prefecture, 1-1, Gakuen-cho, Sakai, Osaka 593, Japan*

Received 2 September 1992; revised 14 December 1992

The multicomponent hydrogen storage alloy with composition $MmNi_{3.31}Mn_{0.37}Al_{0.28}Co_{0.64}$ was used as a negative electrode material. After packing the alloy particles in a porous nickel substrate, press forming was carried out to bond them. The effects of particle size and forming pressure on electrode performance were examined in 6 M KOH solution. The electrochemical properties of the negative electrode, such as discharge capacity and high-rate dischargeability, were remarkably improved by increasing the alloy particle size and forming pressure.

## 1. Introduction

Nickel–hydrogen batteries employing hydrogen storage alloys as a negative electrode material have several inherent advantages over conventional nickel–cadmium batteries with respect to storage capacity, cleanness, and tolerance to overcharging and overdischarging [1, 2]. In recent years, extensive research and development of rechargeable batteries of this type, directed toward practical use, have been carried out [3–7]. In general, the characteristics of negative electrodes were affected by the composition and preparation conditions of the alloy and also by the forming conditions of the electrode. In this work, a nonstoichiometric $AB_{4.6}$ compound, i.e. $MmNi_{3.31}Mn_{0.37}Al_{0.28}Co_{0.64}$ alloy, was employed as a negative electrode material because of its improved discharge capacity and long cycle life [8]. The effects of the particle size and the electrode forming pressure on the charge and discharge performance were investigated.

## 2. Experimental details

$MmNi_{3.31}Mn_{0.37}Al_{0.28}Co_{0.64}$ alloy was separated into two particle sizes of 20–25 $\mu$m and 106–125 $\mu$m by passing through sieves after mechanical pulverization. Negative electrodes were prepared by the following procedure. After mixing the alloy particles (100 mg) with a small amount of polyvinyl alcohol (PVA) solution, the mixture was poured into porous nickel substrate (1.0 cm × 2.5 cm) and then dried in vacuum before pressing at different pressures ranging from 100 to 2000 kg cm$^{-2}$. A glass cell with three compartments separated by sintered glass was employed for the electrochemical measurements. The negative electrode was placed in the central compartment with the two positive electrodes consisting of sintered nickel hydroxide in compartments on each side. The electrochemical capacity of the positive electrodes was designed to be sufficiently larger than that of the negative electrode. A Hg/HgO 6 M KOH electrode was employed as reference. All electrode potentials are given with respect to this reference electrode. The electrolyte was deaerated 6 M KOH solution. Galvanostatic charge–discharge cycling tests were performed at 30 °C under the unpressurized condition. A negative electrode having 100 mg of hydrogen storage alloy was charged for 2.5 h and discharged to −0.5 V against Hg/HgO, both at 20 mA. Between the charging and discharging processes, the current was interrupted for 10 min. Such a cycle was repeated by using a galvanostatic charge–discharge unit (HJ-201, Hokuto Denko).

High-rate dischargeability was determined from the ratio of the discharge capacity at 200 mA to the total capacity that was assumed to be the sum of the discharge capacity at 200 mA, ($C_{200}$) and the additional capacity at 20 mA ($C_{20}$). The latter capacity was determined after the measurement of the former by resting the electrode for 10 min. The high-rate dischargeability was defined as follows:

$$\text{High–rate dischargeability (\%)} = C_{200} \times 100/(C_{200} + C_{20}) \quad (1)$$

High-rate chargeability was evaluated from the discharge capacity at 20 mA after charging at

0021-891X  

200 mA up to a depth of 100% ($C'_{200}$). It was then calculated by the following equation:

$$\text{High-rate chargeability (\%)} = C'_{200} \times 100/C'_{20} \quad (2)$$

where $C'_{20}$ is the discharge capacity at 20 mA after charging at 20 mA for 2.5 h.

Impedance measurement was carried out using a frequency analyser (NF Electronic Instruments 5010 type) in conjunction with a potentiostat (Hokuto Denko, HA-501). The frequency was scanned stepwise from 10 kHz to 0.1 Hz under potentiostatic conditions. Each freshly prepared electrode was activated by ten charge–discharge cycles, and the depth of charge was kept at 100%.

Surface morphology was characterized by scanning electron microscopy (SEM). Pressure-composition isotherms for $MmNi_{3.31}Mn_{0.37}Al_{0.28}Co_{0.64}$ powder-H system were measured by Sieverts' method. The amount of hydrogen storage ($C_H$) was evaluated from $P$–$C$–$T$ data by the following equation:

$$C_H(\text{mAh g}^{-1}) = 5.6 \times 1000F \times \{(H/M)_{0.5} - (H/M)_{0.01}\}/3600MW \quad (3)$$

where $H/M$ is atomic ratio of hydrogen to metal, the subscript indicates hydrogen pressure (in MPa) and $F$ and $MW$ are the Faraday constant and the molecular weight of the hydrogen storage alloy, respectively.

## 3. Results and discussion

### 3.1. Discharge capacity

Pressure-composition isotherms were measured at various temperatures and the results are shown in Fig. 1. The calculated capacity has a maximum value of about 271 mAh g$^{-1}$ at a temperature around 30 °C. Therefore, all electrochemical measurements were performed at 30 °C.

Figure 2 shows the typical capacity build up of the negative electrodes as a function of cycle number. Within a few cycles, discharge capacity levelled off and reached a saturation value depending on the particle size and forming pressure. The saturation capacity increased with increasing particle size and forming pressure. This fact indicates that the efficiency of microcurrent collection is improved by employing alloy of large particle size and high forming pressure. The maximum saturation capacity was found to be 270 mAh g$^{-1}$ for the negative electrode consisting of an alloy with a particle size of 106–125 μm and press-formed at 1200 kg cm$^{-2}$.

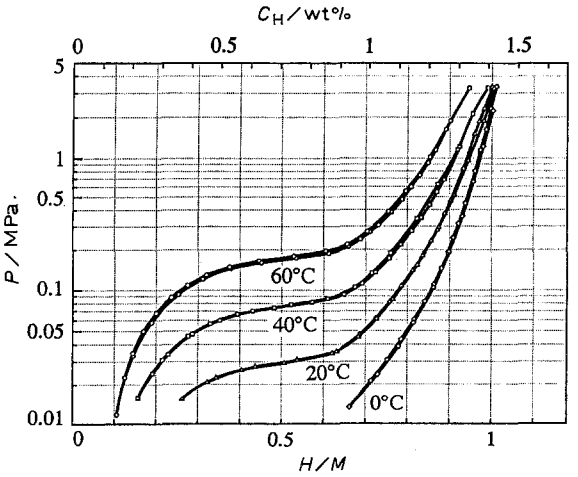


Fig. 1. Pressure-composition isotherms at 0, 20, 40 and 60 °C.

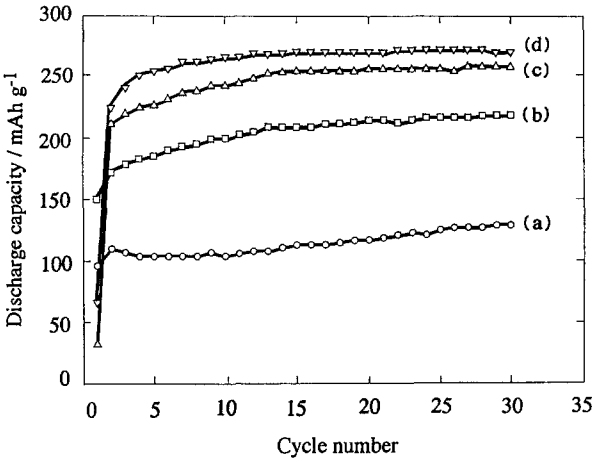


Fig. 2. Discharge capacity as a function of cycle number. (a) 20–25 μm, 200 kg cm$^{-2}$; (b) 20–25 μm, 1200 kg cm$^{-2}$; (c) 106–125 μm, 200 kg cm$^{-2}$; (d) 106–125 μm, 1200 kg cm$^{-2}$.

The discharge capacity measured at the first and tenth cycles is shown in Fig. 3 as a function of forming pressure. The discharge capacity increased with increasing forming pressure, as the contact resistance among the particles and the current collector decreased. The smaller the alloy particle size, the higher the first cycle discharge capacity (compare curves a and c). This implies that the effective surface area is significant for the activation of the negative electrode, as pointed out previously [9]. However, with respect to the discharge capacity measured at the tenth cycle, higher discharge capacity was obtained by employing the larger

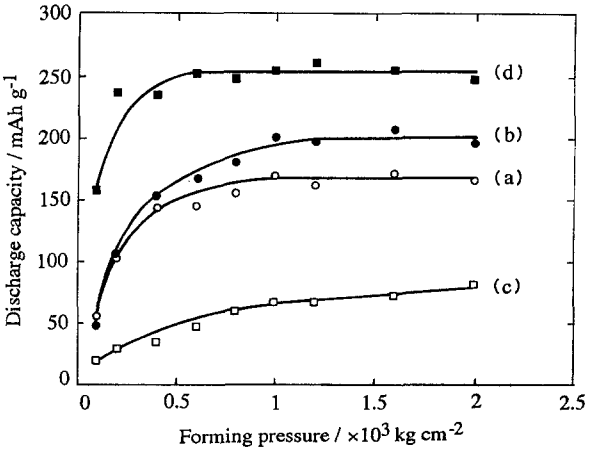


Fig. 3. Discharge capacity of electrodes at the 1st and 10th cycles as a function of forming pressure. (a) 20–25 μm, 1st cycle; (b) 20–25 μm, 10th cycle; (c) 106–125 μm, 1st cycle; (d) 106–125 μm, 10th cycle.

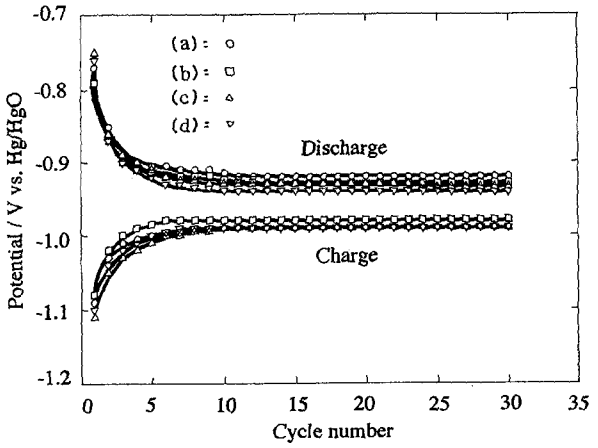


Fig. 4. Steady potential in charge and discharge as a function of cycle number. (a) 20–25 μm, 200 kg cm$^{-2}$; (b) 20–25 μm, 1200 kg cm$^{-2}$; (c) 106–125 μm, 200 kg cm$^{-2}$; (d) 106–125 μm, 1200 kg cm$^{-2}$.

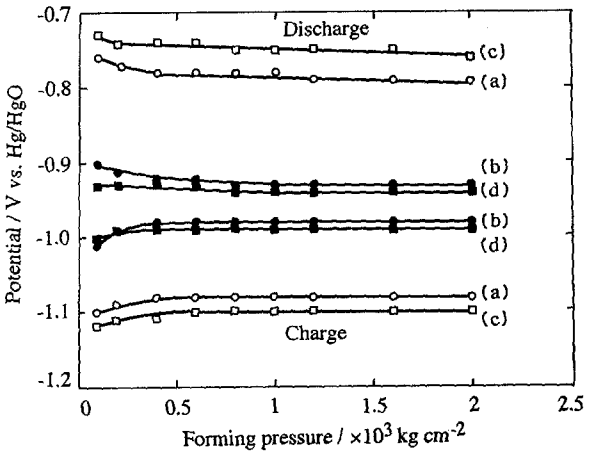


Fig. 5. Steady potential in charge and discharge at the 1st and 10th cycle as a function of forming pressure. (a) 20–25 μm, 1st cycle; (b) 20–25 μm, 10th cycle; (c) 106–125 μm, 1st cycle; (d) 106–125 μm, 10th cycle.

particles. This is probably due to the fact that a new surface having high catalytic activity is produced in an activation process without increasing the contact resistance. The discharge capacity reached a limiting value at forming pressures greater than 600 kg cm$^{-2}$ when alloy particles of size in the range 106–125 μm were employed as negative electrode material. Therefore, the catalytic activity and contact resistance of the alloy particles play an important role in determining the characteristics of the electrode.

### *3.2. Potential of negative electrode in charge and discharge*

The steady charge/discharge potentials of the negative electrode are shown in Fig. 4 as a function of cycle number. The overvoltage in charge and discharge was quite large at the first cycle. The summation of charging and discharging overvoltage amounted to approximately 300 mV or over. As the potential drop, based on the electrolyte resistance, was

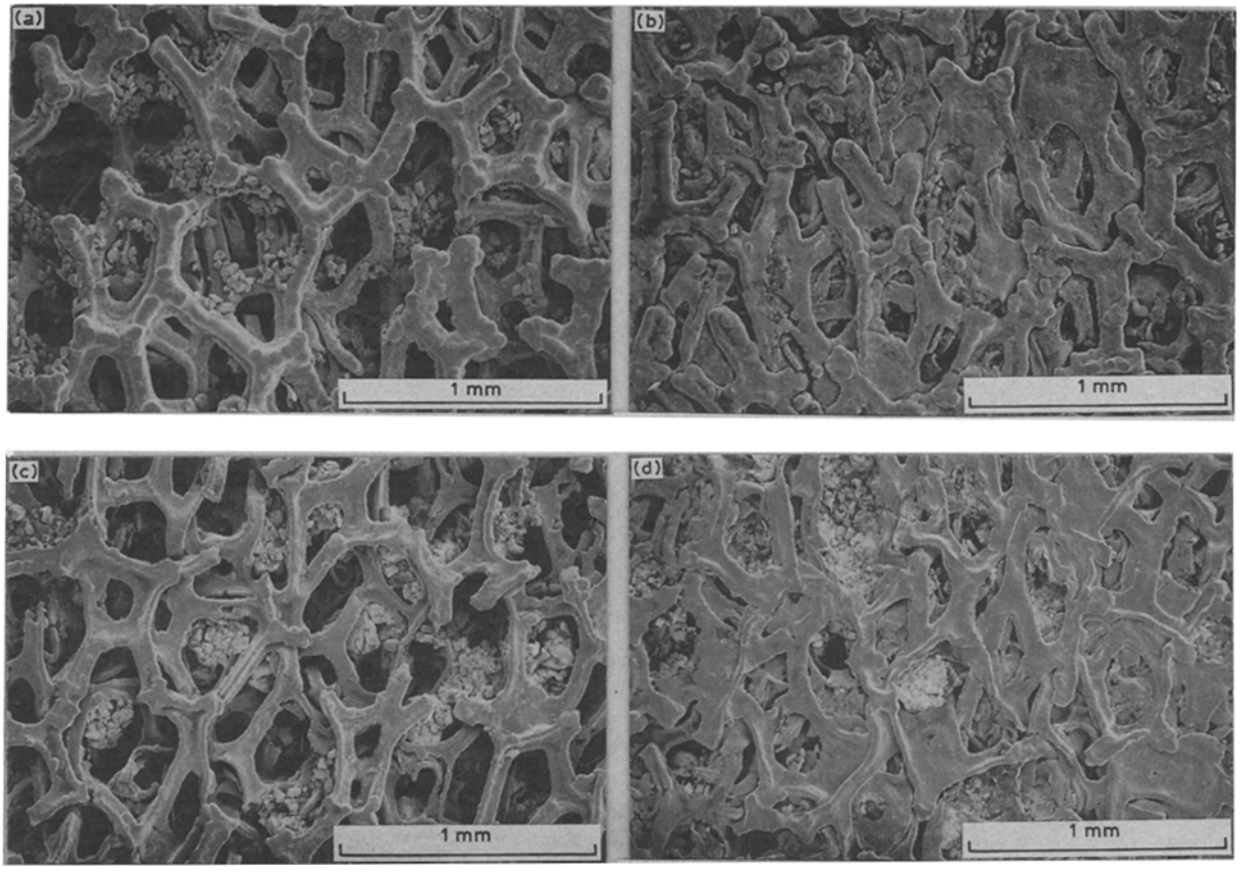


Fig. 6. SEM photographs of the surface of electrodes after cycling. (a) 20–25 μm, 200 kg cm$^{-2}$; (b) 20–25 μm, 1200 kg cm$^{-2}$; (c) 106–125 μm, 200 kg cm$^{-2}$; (d) 106–125 μm, 1200 kg cm$^{-2}$.

*Table 1. Contact resistance and charge-transfer resistance estimated from impedance data by the CNLS fitting algorithm*

| *Particle size/μm* | *Forming pressure/kg cm$^{-2}$* | *Contact resistance/Ω* | *Charge-transfer resistance/Ω* |
|---|---|---|---|
| 20–25 | 200 | 0.16 | 1.06 |
| 20–25 | 1200 | 0.08 | 0.48 |
| 106–125 | 200 | 0.09 | 0.58 |
| 106–125 | 1200 | 0.07 | 0.42 |

assumed to be 4–32 mV, most of the overvoltage was due to charge-transfer resistance or hydrogen diffusion resistance [10]. However, this decreased remarkably to a steady value on repeated charge and discharge cycling, due to the elimination of barrier films such as oxide or absorbed gas.

The potentials of the negative electrode in charge and discharge at the first and tenth cycles are shown (Fig. 5) as a function of forming pressure. The overvoltage at the first cycle was quite large, but it decreased to a limiting value at forming pressures higher than 600 kg cm$^{-2}$. The negative electrode consisting of alloy with particle size in the range 106–125 μm gave a larger overvoltage compared to the smaller particles. This fact is in good agreement with the preceding Section. A similar dependence of overvoltage on forming pressure was observed for the overvoltage measured at the tenth cycle. The limiting overvoltage in charge and discharge at the tenth cycle is almost identical regardless of particle size, nevertheless, the charging and discharging potential shifted slightly in the noble direction for smaller particles.

### *3.3. Surface morphology of negative electode*

Typical SEM photographs of the negative electrode after cycling are shown in Fig. 6. As can be seen from Fig. 6(a)–(d), the effect of forming pressure on the morphology of the negative electrode is considerable. The negative electrodes pressed at 200 kg cm$^{-2}$ had a very porous structure compared to those pressed at 1200 kg cm$^{-2}$. This porous structure resulted in insufficient current collection, leading to the low saturation capacity. The key factor in achieving adequate current collection appeared to be the selection of a particle size comparable to the pore size of the porous nickel substrate. After the charge and discharge cycling test, disintegration of the alloy by crack formation was observed, especially for the alloy with particle size 106–125 μm. A new surface having high catalytic activity, was produced during the process, so that the overvoltage during charge and discharge was sharply reduced and higher discharge capacity was obtained as already described.

### *3.4. Impedance analysis and rate capability in charge and discharge*

Typical impedance diagrams measured at electrodes of different particle size and at different forming pressure are shown in Fig. 7. The impedance data were analysed with the aid of a CNLS fitting algorithm, and thus the contact resistance and the charge-transfer resistance were separated. The results are summarized in Table 1. Both the charge-transfer and contact resistances decreased with increasing forming pressure, and this tendency was particularly significant in the case of electrodes consisting of small particles (20–25 μm). The changes in contact resistance were in good agreement with the results obtained by SEM; the contact resistance decreased with increased forming pressure and particle size. The same tendency was obtained for the charge-transfer resistance. Hence, the forming pressure and the particle size not only affect the contact resistance, but also they affect the charge-transfer resistance. The contact resistance and charge-transfer resistance took a minimum value for the negative electrode made of particles of 106–125 μm and pressed at 1200 kg cm$^{-2}$; therefore, the maximum discharge capacity and the minimum overvoltage was obtained under these conditions.

The results of high-rate dischargeability and chargeability determined at 200 mA are summarized in Table 2. In the case of the electrode consisting of 20–25 μm particles, the high-rate dischargeability increased with increasing forming pressure. However, in the case of larger alloy particles of 106–125 μm, the effect of forming pressure was insignificant. At the lower forming pressure, the

*Table 2. Effects of particle size and forming pressure on rate capability at 200 mA in charging and discharging*

| *Particle size/μm* | *Forming pressure/kg cm$^{-2}$* | *Rate capability* | |
|---|---|---|---|
| | | Discharge/% | Charge/% |
| 20–25 | 200 | 67.7 | 92.1 |
| 20–25 | 1200 | 77.2 | 93.2 |
| 106–125 | 200 | 75.3 | 91.5 |
| 106–125 | 1200 | 76.3 | 92.4 |

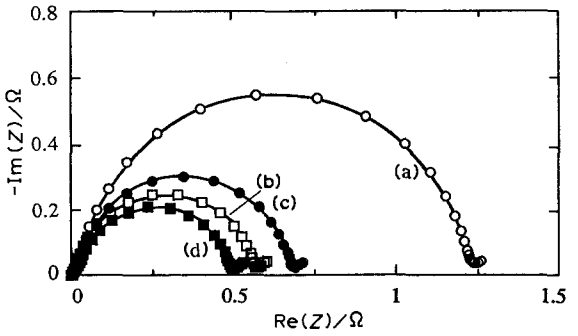


Fig. 7. Typical impedance diagrams of electrodes. (a) 20–25 $\mu$m, 200 kg cm$^{-2}$; (b) 20–25 $\mu$m, 1200 kg cm$^{-2}$; (c) 106–125 $\mu$m, 200 kg cm$^{-2}$; (d) 106–125 $\mu$m, 1200 kg cm$^{-2}$.

larger particle size resulted in improved high-rate dischargeability, but the size-effect was not detected at the higher forming pressure.

The high-rate chargeability increased slightly with increasing forming pressure and with decreasing particle size. The influence of these two factors was insignificant, and the value of high-rate chargeability ranged from 91.5% to 93.2%. These values are much higher than the corresponding dischargeability ranging from 67.7% to 77.2%. As pointed out previously [10], the low value of high-rate dischargeability was ascribed to the overvoltage induced by charge-transfer resistance and by hydrogen diffusion delay. In any case, the dischargeability must be improved further for practical use.

**Acknowledgement**

The authors are indebted to Dr K. Oguro and Dr N. Kuriyama, Government Industrial Research Institute, Osaka, for obtaining *P–C–T* data and for impedance analysis.

**References**

[1] C. Iwakura and M. Matsuoka, *Prog. Batteries & Battery Materials*, **10** (1992) 81.
[2] C. Iwakura and M. Matsuoka, *Kidorui* (*Rare Earth*), No. 17, (1990) pp. 11-36.
[3] J. J. G. Willems and K. H. J. Buschow, *J. Less-Common Met.* **129** (1987) 13.
[4] H. Ogawa, M. Ikoma, H. Kawano and I. Matsumoto, Proc. 16th International Power Sources Symposium, Bournemouth, UK (1988) p. 393.
[5] Y. Moriwaki, T. Gamo, A. Shintani and T. Iwaki, *Denki Kagaku* **57** (1989) 488.
[6] M. A. Fetcenko, S. R. Ovshinsky, S. Venkatesan, K. Kajita, H. Kidou and K. Jeffries, Third International Rechargable Battery Seminar, Florida, USA (1990).
[7] T. Saki, A. Takagi, H. Miyamura, N. Kuriyama, H. Ishikawa and C. Iwakura, Proc. 3rd International Conference on Batteries for Utility Energy Storage (1991) p. 499.
[8] N. Nogami, K. Moriwaki and N. Furukawa, Third International Rechargable Battery Seminar, Florida, USA (1990).
[9] M. Matsuoka, H. Mori, K. Asai and C. Iwakura, *Chem. Express* **7** (1992) 189.
[10] C. Iwakura, M. Matsuoka, K. Asai and T. Kohno, *J. Power Sources* **38** (1992) 335.